

## Synthesis and Application of Fe<sub>3</sub>O<sub>4</sub>/SiO<sub>2</sub>/TiO<sub>2</sub> Nanocomposite as a Photocatalyst in CO<sub>2</sub> Indirect Reduction to Produce Methanol

Yudha Ramanda, Nuryono, and Eko Sri Kunarti\*

Department of Chemistry, Faculty of Mathematics and Natural Sciences, Universitas Gadjah Mada, Sekip Utara BLS 21, Bulaksumur, Yogyakarta 55281, Indonesia

\* Corresponding author:

email: eko\_kunarti@ugm.ac.id

Received: July 31, 2017

Accepted: April 2, 2019

DOI: 10.22146/ijc.27079

**Abstract:** This study focuses on the synthesis and application of a Fe<sub>3</sub>O<sub>4</sub>/SiO<sub>2</sub>/TiO<sub>2</sub> nanocomposite as a photocatalyst in CO<sub>2</sub> indirect reduction. The synthesis was started by preparation of magnetite (Fe<sub>3</sub>O<sub>4</sub>) followed by silica (SiO<sub>2</sub>) coating and titania (TiO<sub>2</sub>) deposition. Magnetite was prepared by the sono-coprecipitation method, then the coating of SiO<sub>2</sub> and deposition of TiO<sub>2</sub> were performed by the sol-gel method under ultrasonic irradiation. All the material products were characterized by an X-ray diffractometer (XRD), Fourier-transform infrared spectrophotometer (FTIR), and transmission electron microscope (TEM). The final material product was also analyzed by a specular reflectance UV-Visible spectrometer (SR-UV-Vis) and the turbidimetry method. The product of the indirect reduction was analyzed by a gas chromatography-mass spectrometer (GC-MS). The XRD diffractograms and FTIR spectra confirmed the presence of Fe<sub>3</sub>O<sub>4</sub>, SiO<sub>2</sub>, and the anatase phase of TiO<sub>2</sub>. The TEM images revealed the presence of a core-shell nanocomposite with an average diameter of 19.22 ± 1.25 nm. The SR-UV-Vis spectrum was used to determine the band gap energy of the photocatalyst, with the result being 3.22 eV. Turbidimetry aimed to measure the magnetic recoverability of the final material, and the result was that it had better recoverability compared to a non-magnetic photocatalyst composite. The GC chromatogram of the indirect reduction product indicated four major fractions; the MS spectra showed these to be methanol, formaldehyde, formic acid, and CO<sub>2</sub>. The GC-MS results revealed that CO<sub>2</sub> indirect reduction achieved 73.91% conversion of CO<sub>2</sub> and 55.01% selective to methanol.

**Keywords:** Fe<sub>3</sub>O<sub>4</sub>/SiO<sub>2</sub>/TiO<sub>2</sub>; indirect reduction; nanocomposite; photocatalyst

### ■ INTRODUCTION

During this decade, the effects of climate change caused by atmospheric CO<sub>2</sub> have become a hot issue [1]. A core ice expedition revealed that CO<sub>2</sub> concentration in the atmosphere had reached a steady state until the industrial revolution [2-4]. Subsequently, this concentration significantly increased, with an exponential 2.5% growth rate trend. This situation has already reached two-thirds of the critical value. Up to 1,430 gigatons/year of CO<sub>2</sub> were released from 1870 to 2013, a figure which is predicted to increase to 1,670 gigatons/year by 2019 [1]. This state has motivated the research of transforming CO<sub>2</sub> into valuable materials to limit its concentration in the atmosphere [5-7]. CO<sub>2</sub> can be used as a carbon feedstock

to synthesize various useful chemicals such as alcohol, carboxylic acid, and aldehyde. These chemicals can also be used to synthesize others, such as nitrile, ester, imine, and amide. Gomes et al. [8] developed reactions and catalysts to utilize CO<sub>2</sub> as a carbon feedstock to substitute for petrochemical feedstock.

Other studies have dealt with the transformation of CO<sub>2</sub> into fuel, either methanol fuel or natural gas [9-10]. These actions are being taken to resolve another problem, the energy crisis. Energy is a primary need to support civilization. Several sectors, such as industry, hospitality, and education, depend on energy supplies. If CO<sub>2</sub> becomes a form of energy supply, its concentration in the atmosphere will significantly decrease because energy demand is huge, up to 13,541 Mtoe [11]. At

present, 81% of energy is provided by fossil fuel, with only 13% coming from renewable resources [12]. This situation increases the CO<sub>2</sub> releasing rate. Another estimation reveals that renewable resources, apart from solar energy, only have a capacity of up to 20 TW, while the prediction for energy demand in 2050 is up to 27 TW. This means that the renewable resource with the most potential is solar energy. However, this has a critical weakness, which is its low energy density. To solve this problem, solar energy can be stored in the form of chemical energy, such as methanol. Methanol has a liquid phase, which makes it easier to handle than solar energy radiation. Methanol also has a higher energy density, caused by the high energy bond in the C-H bond. The problem is that CO<sub>2</sub> has higher thermodynamic stability than methanol, which means the transformation of CO<sub>2</sub> into methanol needs external energy as the driving force.

The CO<sub>2</sub> gas can be transformed into fuel with a reductive pathway [13]. Some studies have used direct reduction from CO<sub>2</sub> into methanol or methane [9,14]. However, direct reduction produces a small yield because CO<sub>2</sub> is thermodynamically stable. To handle this issue, our group developed photocatalyst assisted reduction under UV irradiation as external energy that acts as a driving force in CO<sub>2</sub> reduction.

Besides, the sustainable catalyst must have a good recovery system, such as magnetic recovery system. The heterogeneous magnetic catalyst has good recoverability property that enhanced the sustainability of catalyst [15]. This property was perfectly matched with photocatalyst because photocatalysis occurs in a heterogeneous system where this property enhances the recovery of the photocatalyst. The magnetic photocatalyst reduction was studied in our former research [16-17], gave a good result in metal photoreduction under UV irradiation. The others [18-19] even responsive to visible light in metal photoreduction.

Meanwhile, the application into organic matter is limited in number. One of the application was photocracking of carboxymethyl cellulose to produce biofuel in ambient condition [15] but almost none in organic photoreduction. In this article, the photoreduction of CO<sub>2</sub> with carbonate as an intermediate

was discussed.

This research has developed an indirect reduction of CO<sub>2</sub> by utilizing nanocomposite photocatalyst as an electron generator. The concept of indirect reduction is not to reduce CO<sub>2</sub>, but reducing carbonate ion instead. The CO<sub>2</sub> can be transformed into carbonate ion by dissolving in acidic solution. The carbonate ion is easier to handle than CO<sub>2</sub> gas and also easier to encounter with the catalyst surface. The aqueous solution has H<sub>2</sub>O and H<sup>+</sup> that can be used as an electron scavenger to enhance electron mobility. The photocatalyst that is used in this research was designed for continuous aqueous reaction with magnetic recoverability system. In this work, the magnetic recoverability photocatalyst (Fe<sub>3</sub>O<sub>4</sub>/SiO<sub>2</sub>/TiO<sub>2</sub>) was tested to reduce CO<sub>2</sub> in the indirect reductive pathway with carbonate ion as intermediate.

## ■ EXPERIMENTAL SECTION

### Materials

The analytical grade reagents purchased from Merck were iron(II) sulfate heptahydrate (FeSO<sub>4</sub>·7H<sub>2</sub>O), iron(III) chloride hexahydrate (FeCl<sub>3</sub>·6H<sub>2</sub>O), ammonium hydroxide solution 25% (NH<sub>4</sub>OH), calcium hydroxide (Ca(OH)<sub>2</sub>), sodium citrate dihydrate (Na<sub>3</sub>C<sub>6</sub>H<sub>5</sub>O<sub>7</sub>·2H<sub>2</sub>O), ammonium sulphate ((NH<sub>4</sub>)<sub>2</sub>SO<sub>4</sub>), and sulphuric acid 98% (H<sub>2</sub>SO<sub>4</sub>). Other technical grade reagents purchased from Sigma-Aldrich were titanium isopropoxide 97% (TTIP) and tetraethyl orthosilicate 98% (TEOS). A further technical reagent purchased from Merck was methanol 95% (CH<sub>3</sub>OH).

### Instrumentation

The FTIR spectra were recorded on a Shimadzu Prestige-21 FTIR spectrophotometer with the KBr pellet method, while the XRD diffractograms were recorded on a Shimadzu XRD 6000. The SR-UV-Vis spectrum was recorded on a Pharmaspec UV 1700 spectrophotometer; meanwhile, the turbidimetry was carried out on a Shimadzu UV 1800 spectrophotometer. The GC chromatogram and MS spectra were recorded on a Shimadzu QP-2010S gas chromatography-mass spectrometer. The TEM images were recorded on a JEOL JEM-1400 transmission electron microscope.

Sonication was run on a Bransonic CPX2800H ultrasonic cleanser and calcination was run in a Vulcan A-130 furnace. The other additional equipment included 3 cm × 2 cm × 0.5 cm of permanent ferrite magnet (0.2 Tesla) and Philips TUV TL Mini (UV C,  $\lambda = 253.7$  nm) UV lamp.

## Procedure

### Synthesis of $Fe_3O_4$ nanoparticle

As much as 6.02 g of  $FeCl_3 \cdot 6H_2O$  and 4.08 g of  $FeSO_4 \cdot 7H_2O$  were dissolved in 60 mL of ion-free water and then aerated with  $N_2$  gas during the synthesis. The solution was stirred, and a 25%  $NH_4OH$  solution was added dropwise until the pH was 10; the mixture was then sonicated for 1 h until a black precipitate was formed. This formed precipitate was then separated by an external magnet and washed until the pH was 7. The precipitate was soaked in 100 mL of sodium citrate 0.2 M solution overnight. Subsequently, the precipitate was washed until the pH was 7 and desiccated overnight. The prepared solid was characterized by XRD, FTIR, and TEM. These procedures based on our former paper [16] with modification to produce nanoparticle.

### Synthesis of $Fe_3O_4/SiO_2$

An amount of 0.1 g of  $Fe_3O_4$  was soaked in 60 mL of technical grade methanol. The mixture was stirred, and 1 mL of TEOS was added; the mixture was then sonicated for 3 h. Next, the solid was separated by an external magnet and desiccated overnight. The as-prepared solid was characterized by XRD, FTIR, and TEM.

### Synthesis of $Fe_3O_4/SiO_2/TiO_2$

The  $Fe_3O_4/SiO_2$  (0.1 g) was immersed in 60 mL of technical grade methanol. The mixture was blended, and 1 mL of TTIP was added; the mixture was then sonicated for 3 h. Next, the solid was removed from the mixture by an external magnet and desiccated overnight. The as-prepared solid was calcined at 500 °C for 4 h. The prepared solid was characterized by XRD, FTIR, and TEM.

### Indirect reduction

One hundred milliliters of  $H_2SO_4$  2 M was aerated with  $CO_2$  for 1 h. The solution of  $Ca(OH)_2$  0.5 M was added into the previous solution until the pH was 6.3, and 50 mg  $Fe_3O_4/SiO_2/TiO_2$  was added. The mixture was

illuminated with a UV lamp ( $\lambda = 253.7$  nm) for 1 h. The solid was separated by an external magnet, and the solution was analyzed by GC-MS.

### Reusability and magnetic recoverability

Ten milliliters of feed ( $CO_2$  in  $H_2SO_4$  solution) was added to 50 mg of  $Fe_3O_4/SiO_2/TiO_2$ . The mixture was illuminated with UV radiation ( $\lambda = 253.7$  nm) for 30 min. Before the solid was separated from the mixture, the absorbance of the mixture was measured with a UV-Vis spectrophotometer, and the solid was then separated by an external magnet. After a cycle, the solid was soaked in 10 mL of fresh feed and run for a further ten catalytic cycles. Each product from a catalytic cycle was analyzed to determine the concentration of  $CO_2$ .

### Turbidimetry method

A sufficient amount of material was taken and dispersed with ultrasonic irradiation in methanol to make a 1 ppm mixture. The absorbances of the mixture were measured under a 0.2 Tesla magnetic field by 3 cm × 2 cm × 0.5 cm of permanent ferrite magnet. The measurement was examined on Shimadzu UV 1800 spectrophotometer (real-time mode) and plotted against time to give a turbidimetry diagram. This method based on the research of Baran et al. [20] about the stability of magnetic photocatalyst measured by the turbidimetric method.

## RESULTS AND DISCUSSION

### Synthesis of the $Fe_3O_4/SiO_2/TiO_2$ Nanocomposite

The  $Fe_3O_4/SiO_2/TiO_2$  composite has three components: a magnetic core, silica barrier, and titania deposit. The magnetic core will enhance the recovery system with an external magnetic field to make the composite easier to recover. Titania embedded in the composite acts as a semiconductor to give photocatalytic activity under UV irradiation. The purpose of the silica barrier is to improve the magnetite solvent stability and to prevent self-oxidation by photocatalyst (photodissolution) by avoiding contact between the magnetic core and titania deposit. In this research, the material was developed by decreasing the particle size to produce a nanomaterial, which will have higher photocatalytic activity.

The FTIR spectra and XRD diffractograms (Fig. 1) confirm the presence of  $\text{Fe}_3\text{O}_4$  (M),  $\text{SiO}_2$  (S), and the anatase phase of  $\text{TiO}_2$  (A) with a composite trend in which the component signal (peaks for the FTIR spectrum and intensity for the XRD diffractogram) co-exist. FTIR spectrum (a) indicates the appearance of  $\text{Fe}_3\text{O}_4$  from Fe-O vibration around  $500\text{ cm}^{-1}$ . This is proven by diffractogram (a), in which there are specific peaks of magnetite. FTIR spectrum (b) indicates the co-existence of  $\text{Fe}_3\text{O}_4$  and  $\text{SiO}_2$ . Evidence for this is the absorbance of Fe-O vibration around  $500\text{ cm}^{-1}$  and the absorbance of Si-O vibration around  $1100\text{ cm}^{-1}$ . These vibrations exist together and indicate composite occurrences. This is also proven by diffractogram (b), which indicates the same trend in which magnetite specific peaks and amorphous  $\text{SiO}_2$  broad peak co-exist. FTIR spectrum (c) gives the composite trend from the absorbance of Fe-O vibration, the absorbance of Si-O vibration, and absorbance of Ti-O (around  $500\text{ cm}^{-1}$ ). This evidence is also proven by

diffractogram (c), which indicates the composite trend in which magnetite specific peaks, silica broad peak, and anatase phase of  $\text{TiO}_2$  specific peaks co-exist.

The TEM images (Fig. 2) reveal the nanocomposite structure with a core-shell structure. Fig. 2(a) shows a spherical solid with an average diameter of  $8.95 \pm 0.88\text{ nm}$ . This image proves that sodium citrate as a capping agent worked to limit the crystal growth of  $\text{Fe}_3\text{O}_4$  and produced a nanomaterial specific to nanoparticle material. Fig. 2(b) shows the mass with a spherical-like structure and an average diameter of  $11.20 \pm 1.09\text{ nm}$ . In this mass, there are two main gradations, a darker spherical particle, and brighter shade. The shade coated the particle, and the image indicates the appearance of a coated material.  $\text{Fe}_3\text{O}_4$  is denser than amorphous silica, which would mean that the TEM image of  $\text{Fe}_3\text{O}_4$  should be darker than that of amorphous silica. The conclusion is that the particle should be  $\text{Fe}_3\text{O}_4$  and the shade should be amorphous silica. Fig. 2(b) can be interpreted as a composite of  $\text{Fe}_3\text{O}_4/\text{SiO}_2$ .

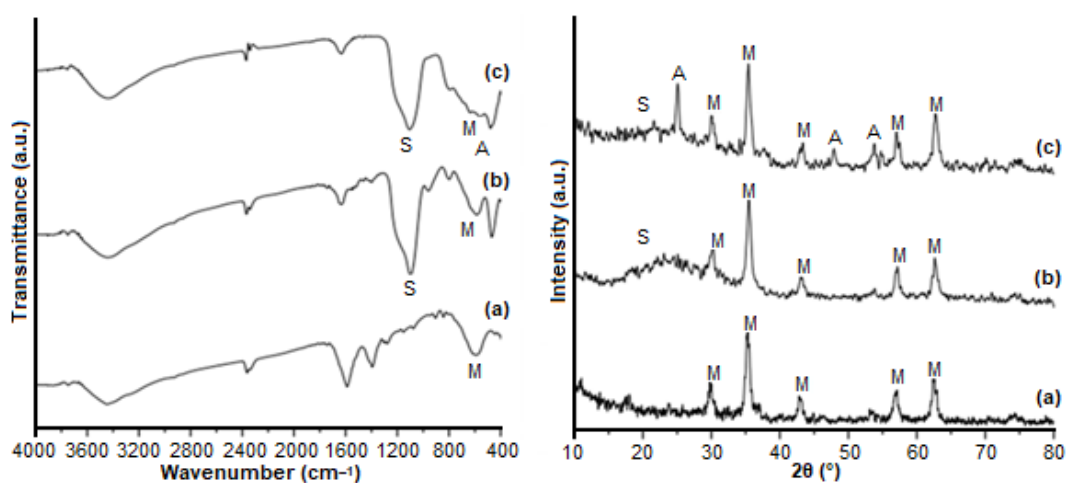


Fig 1. FTIR spectra (left) and XRD diffractograms (right) of (a)  $\text{Fe}_3\text{O}_4$ , (b)  $\text{Fe}_3\text{O}_4/\text{SiO}_2$  and (c)  $\text{Fe}_3\text{O}_4/\text{SiO}_2/\text{TiO}_2$

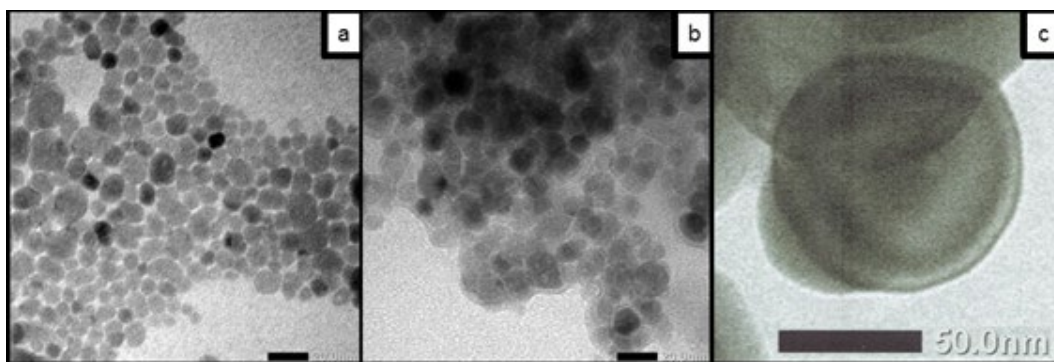


Fig 2. TEM images of (a)  $\text{Fe}_3\text{O}_4$ , (b)  $\text{Fe}_3\text{O}_4/\text{SiO}_2$  and (c)  $\text{Fe}_3\text{O}_4/\text{SiO}_2/\text{TiO}_2$

Fig. 2(c) shows a spherical particle that has an average diameter of  $19.22 \pm 1.25$  nm. This particle has a dark-bright-dark pattern, indicating a three-layer composite. Both  $\text{Fe}_3\text{O}_4$  and  $\text{TiO}_2$  are denser than amorphous silica. The study concludes that the dark core is  $\text{Fe}_3\text{O}_4$ , the bright one should be amorphous silica, and the dark color on the material surface should be  $\text{TiO}_2$ . The final material also had a diameter of less than a hundred nanometer and can be concluded to be the  $\text{Fe}_3\text{O}_4/\text{SiO}_2/\text{TiO}_2$  nanocomposite.

The TEM image of the  $\text{Fe}_3\text{O}_4$  shows a spherical structure. The average diameter of the mass in the TEM image increased during component lamination. These facts indicate that the nanomaterial has a spherical structure at the beginning and then produces the nanocomposite with a core-shell structure, with  $\text{Fe}_3\text{O}_4$  as the magnetic core and an amorphous silica coat with the deposition of  $\text{TiO}_2$  as the shell. The core-shell structure was preferred because the template ( $\text{Fe}_3\text{O}_4$  nanoparticle) has a spherical structure, as seen in Fig. 2(a). This phenomenon was also observed by Liu et al. [21].

Other evidence is provided by the turbidimetry diagram (Fig. 3), which shows that the magnetic recoverability decreases with the addition of more components.  $\text{SiO}_2/\text{TiO}_2$  worked as a blank in this measurement. The different absorbances indicate different magnetic property. This different magnetic property indicates lamination onto the template surface instead of aggregation. If each component aggregates by itself, the magnetic property of each material will be the same because the magnetic component will create different aggregate from the other components. In this study,  $\text{Fe}_3\text{O}_4$  worked as a template and core of the composite. The composite could be a nanocomposite with a core-shell structure.

### Study of Photocatalytic Activity

Fig. 4 shows a comparison between the direct and indirect reduction routes. Direct reduction needs a porous material as a support material because in this route the reactants were  $\text{CO}_2$  gas and syngas (a mixture of CO and  $\text{H}_2$ ). To enhance the catalyst-substrate encounter, the support material needs to be porous so that it can adsorb the reactant. Indirect reduction does not need a

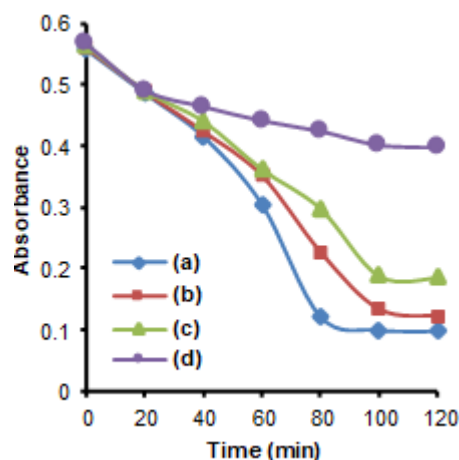


Fig. 3. Turbidimetry diagram of (a)  $\text{Fe}_3\text{O}_4$ , (b)  $\text{Fe}_3\text{O}_4/\text{SiO}_2$ , (c)  $\text{Fe}_3\text{O}_4/\text{SiO}_2/\text{TiO}_2$  and (d)  $\text{SiO}_2/\text{TiO}_2$

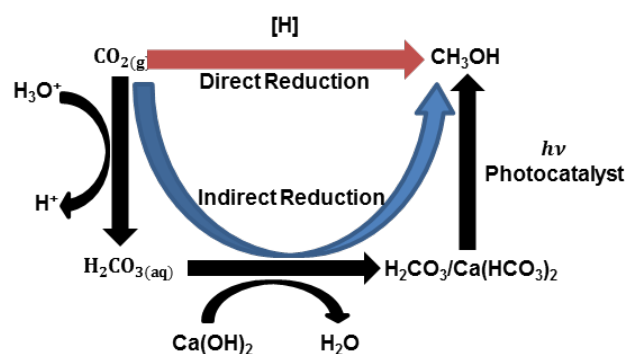


Fig. 4. Scheme of direct-indirect reduction route comparison

porous support material because the reactants have better mobilization in the aqueous solution as carbonate ion, nor does it need syngas as a reducing agent because the electrons generated by the photocatalyst can trigger water photolysis, which produces hydrogen as a reducing agent (in this case, the hydrogen radical).

The photocatalytic activity of the  $\text{Fe}_3\text{O}_4/\text{SiO}_2/\text{TiO}_2$  nanocomposite was evaluated specifically for indirect reduction of  $\text{CO}_2$ . The  $\text{CO}_2$  was trapped in an acidic solution as carbonic acid ( $\text{H}_2\text{CO}_3$ ) under an acid-catalyzed dissolution and was added by some basic solution to form a bicarbonate buffer system in order to adjust the pH to 6.3. If the solution were too acidic, the material would lose the anatase phase of  $\text{TiO}_2$  because of reversible acid-catalyzed hydrolysis of  $\text{TiO}_2$  and loss of photocatalytic activity. If the solution were too basic, the photoreduction mechanism would be distracted by

hydroxyl radical generation, leading to the photooxidation mechanism becoming more dominant. To avoid the domination of photooxidation, the solution was also pre-treated by aerating with  $N_2$  gas to remove the dissolved oxygen from it. Dissolved oxygen may induce photooxidation caused by oxygen radical generation. Zuas et al. [22] conducted  $CO_2$  photoreduction under basic conditions and obtained methanol as a minor product, and the major products were unidentified products.

In indirect reduction, water hydrolysis will undergo coupled carbonate reduction to produce methanol and will produce protons. Protons can act as electron scavengers to transfer electrons from the photocatalyst surface to the substrate. This process makes the reduction by photocatalyst easier and will improve product conversion. Dissolution of  $CO_2$  also stabilizes intermediate species and makes electron transfer more efficient. The direct route needs porous support selective to adsorb  $CO_2$  and easy to remove the product from the catalyst surface. The indirect route, however, does not need this because the products and reactants have good mobility in the aqueous solution and will find it easier to encounter the photocatalyst surface.

The product of the indirect reduction was analyzed by GC-MS, and the resulted chromatogram is shown in Fig. 5 (MS spectra and discussion available in supplementary S1). Table 1 shows that the three products of the indirect reduction are formic acid, formaldehyde, and methanol (major). This indicates the step-by-step reduction. The oxidation level of the product component leads to the deduction that the carbonate will be reduced to formic acid; formic acid will be reduced to formaldehyde, and formaldehyde will be reduced to methanol. The product percentages are not equal, indicating that each step has a different rate of production. This means that electron transfer and the kinetic challenge in each step are not the same. If they had

the same challenge, the product concentration would not be significantly different. As can be seen, the reduction of carbonate to formic acid is the biggest challenge and gives a lowest product. The other reasons are that the reduction of formic acid to formaldehyde, and the reduction of formaldehyde to methanol, are easier than the reduction of carbonate to formic acid, which makes the rate of formic acid consumption greater than the rate of formic acid production. These phenomena show that the biggest challenge is to convert carbonate to formic acid. Table 1 shows that an indirect reduction of  $CO_2$  had been achieved, with 73.91% conversion of  $CO_2$  and 55.01% selective to methanol.

Habisreutinger et al. [23] discovered that a common metal oxide photocatalyst could not reduce  $CO_2$  directly to methanol. If another product, consider an intermediate to produce methanol (the lowest carbon oxidation product), the mechanism could be as shown in Fig. 6. The reduction was a step-by-step reduction with a photocatalyst as an electron generator and protons as electron scavengers.

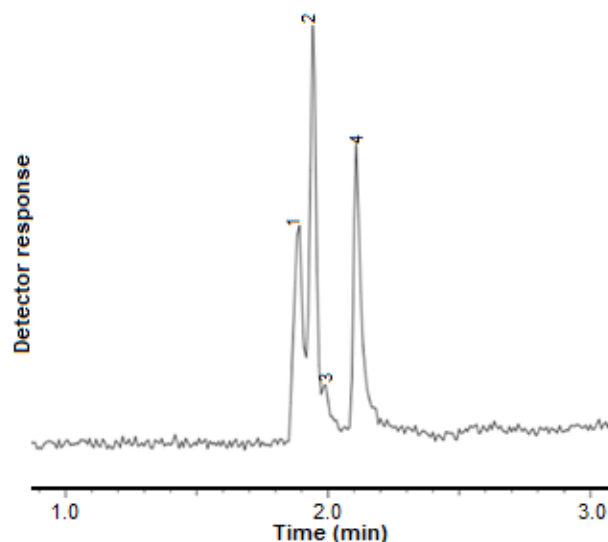


Fig 5. GC chromatogram of indirect reduction product

Table 1. Components of indirect reduction product

Peak number	Retention time (min)	Peak area (%)	MS prediction
1	1.889	29.65	Formaldehyde
2	1.943	40.66	Methanol
3	1.992	3.59	Formic Acid
4	2.108	26.09	$CO_2$

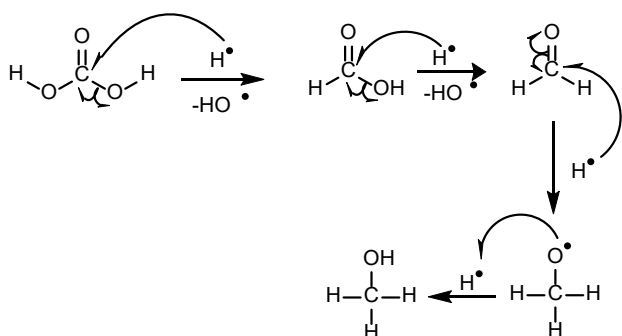


Fig 6. Prediction of the reduction mechanism

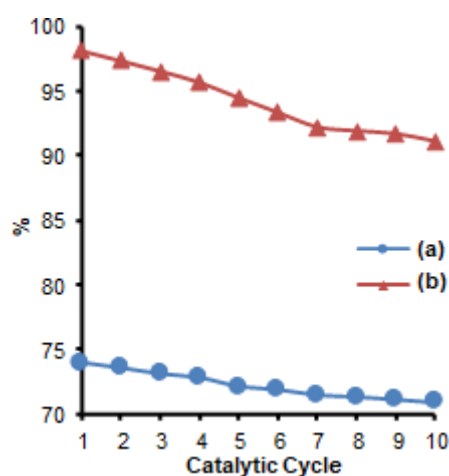


Fig 7. Diagram of (a) % conversion and (b) % recovery

### Magnetic Recoverability and Reusability

Magnetic recoverability and reusability were studied under ten catalytic cycles. As seen in Fig. 7, under these cycles, catalytic activity does not decrease significantly. This trend can be seen from the % conversion diagram (a) that decreases only 5% after ten catalytic cycles. The % recovery (b) is determined by turbidimetry, which measures the absorbance of the substrate after a catalytic cycle. The  $\lambda$  (450 nm) in this method was set to the visible spectrum to avoid photocatalytic reaction during the measurement. This method gave a result of only 10% catalyst mass loss after ten cycles. This result confirms the good magnetic recoverability of the photocatalyst.

### CONCLUSION

$\text{Fe}_3\text{O}_4/\text{SiO}_2/\text{TiO}_2$  nanocomposite had been synthesized and characterized. This material can be used as a photocatalyst for  $\text{CO}_2$  indirect reduction and gives a conversion of 73.91 and 55.01% selective to methanol.

This material also has magnetic recoverability better than the non-magnetic composite according to turbidimetry diagram. The results revealed the indirect reduction of  $\text{CO}_2$  with carbonate ion as intermediate occurs under UV irradiation and have a chance to be improved in further research to be responsive to visible light. Also, the methanol product from indirect photoreduction can be characterized further to check the compatibility as green energy to substitute fossil fuel.

### ACKNOWLEDGMENTS

The authors acknowledge Directorate General of Higher Education, Ministry of Research, Technology, and Higher Education of Republic of Indonesia, Universitas Gadjah Mada, and also the AKUGAMA scholarship (*Beasiswa Alumni Kimia Universitas Gadjah Mada*) for partial financial support.

### REFERENCES

- [1] Friedlingstein, P., Andrew, R.M., Rogelj, J., Peters, G.P., Canadell, J.G., Knutti, R., Luderer, G., Raupach, M.R., Schaeffer, M., van Vuuren, D.P., and Le Quèrè, C., 2014, Persistent growth of  $\text{CO}_2$  emission and implication for reaching climate targets, *Nat. Geosci.*, 7, 709–715.
- [2] Barnola, J.M., Pimienta, P., Raynaud, D., and Korotkevich, Y.S., 1991,  $\text{CO}_2$ -climate relationship as deduced from the Vostok ice core: A re-examination based on a new measurement and on a re-evaluation of the air dating, *Tellus Ser. B*, 43 (2), 83–90.
- [3] Indermühle, A., Monnin, E., Stauffer, B., Stocker, T.F., and Wahlen, M., 2000, Atmospheric  $\text{CO}_2$  concentration from 60 to 20 kyr BP from the Taylor Dome ice core, Antarctica, *Geophys. Res. Lett.*, 27 (5), 735–738.
- [4] Nakazawa, T., Machida, T., Esumi, K., Tanaka, M., Fujii, Y., Aoki, S., and Watanabe, O., 1993, Measurements of  $\text{CO}_2$  and  $\text{CH}_4$  concentrations in air in a polar ice core, *J. Glaciol.*, 39 (132), 209–215.
- [5] Lovell, E.C., Scott, J., and Amal, R., 2015, Ni- $\text{SiO}_2$  catalysts for the carbon dioxide reforming of methane: Varying support properties by flame spray pyrolysis, *Molecules*, 20 (3), 4594–4609.

- [6] Melián-Cabrera, I., Granados, M.L., and Fierro, J.L.G., 2002, Reverse topotactic transformation of a Cu-Zn-Al catalyst during wet Pd impregnation: Relevance for the performance in methanol synthesis from CO<sub>2</sub>/H<sub>2</sub> mixtures, *J. Catal.*, 210 (2), 273–284.
- [7] Vesselli, E., Rizzi, M., de Rogatis, L., Ding, X., Baraldi, A., Comelli, G., Savio, L., Vattuone, L., Rocca, M., Fornasiero, P., Baldereschi, A., and Peressi, M., 2009, Hydrogen-assisted transformation of CO<sub>2</sub> on nickel: The role of formate and carbon monoxide, *J. Phys. Chem. Lett.*, 1 (1), 402–406.
- [8] Gomes, C.D.N., Jacquet, O., Villiers, C., Thuéry, P., Ephritikhine, M., and Cantat, T., 2012, A diagonal approach to chemical recycling of carbon dioxide: Organocatalytic transformation for the reductive functionalization of CO<sub>2</sub>, *Angew. Chem. Int. Ed.*, 51 (1), 187–190.
- [9] Dimitrijevic, N.M., Vijayan, B.K., Poluektov, O.G., Rajh, T., Gray, K.A., He, H., and Zapol, P., 2011, Role of water and carbonates in photocatalytic transformation of CO<sub>2</sub> to CH<sub>4</sub> on titania, *J. Am. Chem. Soc.*, 133 (11), 3964–3971.
- [10] Fu, Y., Sun, D., Chen, Y., Huang, R., Ding, Z., Fu, X. and Li, Z., 2012, An amine-functionalized titanium metal-organic framework photocatalyst with visible-light-induced activity for CO<sub>2</sub> reduction, *Angew. Chem. Int. Ed.*, 51 (14), 3364–3367.
- [11] Richardson, I., Thomson, M., Infield, D., and Clifford, C., 2010, Domestic electricity use: A high-resolution energy demand model, *Energy Build.*, 42 (10), 1878–1887.
- [12] Conti, J., Holtberg, P., Diefenderfer, J., LaRose, A., Turnure, J.T., and Westfall, L., 2016, *International energy outlook 2016 with projections to 2040*, USDOE Energy Information Administration, Washington, 145.
- [13] Fletcher, C., Jiang, Y., and Amal, R., 2015, Production of formic acid from CO<sub>2</sub> reduction by means of potassium borohydride at ambient conditions, *Chem. Eng. Sci.*, 137, 301–307.
- [14] Liu, S., Zhang, H., Xu, Z., Zhong, H., and Jin, H., 2012, Nitrogen-doped carbon xerogel as high active oxygen reduction catalyst for direct methanol alkaline fuel cell, *Int. J. Hydrogen Energy*, 37 (24), 19065–19072.
- [15] Ramanda, Y., Thomas, K., Aziz, S., Mauludi, K., and Kunarti, E.S., 2017, Carboxymethyl cellulose photocracking by magnetic recoverable photocatalyst to produce biofuel in ambient condition, *Chim. Natura Acta*, 5 (2), 90–94.
- [16] Kunarti, E.S., Syoufian, A., Budi, I.S., and Pradipta, A.R., 2016, Preparation and properties of Fe<sub>3</sub>O<sub>4</sub>/SiO<sub>2</sub>/TiO<sub>2</sub> core-shell nanocomposite as recoverable photocatalyst, *Asian J. Chem.*, 28 (6), 1343–1346.
- [17] Kunarti, E.S., Roto, R., Pradipta, A.R., and Budi, I.S., 2017, Fe<sub>3</sub>O<sub>4</sub>/SiO<sub>2</sub>/TiO<sub>2</sub> core-shell nanoparticles as catalyst for Ag(I) ions, *Orient. J. Chem.*, 33 (4), 1933–1940.
- [18] Kunarti, E.S., Kartini, I., Syoufian, A., and Widyandari, K.M., 2018, Synthesis and photoactivity of Fe<sub>3</sub>O<sub>4</sub>/TiO<sub>2</sub>-Co magnetically separable visible light responsive photocatalyst, *Indones. J. Chem.*, 18 (3), 403–410.
- [19] Wahyuni, S., Kunarti, E.S., Swasono, R.T., and Kartini, I., 2018, Characterization and photocatalytic activity of TiO<sub>2</sub>(rod)-SiO<sub>2</sub>-polyaniline nano composite, *Indones. J. Chem.*, 18 (2), 321–330.
- [20] Baran, W., Makowski, A., and Wardas, W., 2005, The separation of catalyst after photocatalytic reactions conducted in the presence of TiO<sub>2</sub>/FeCl<sub>3</sub>/UV, *Chemosphere*, 59 (6), 853–859.
- [21] Liu, J., Xu, J., Che, R., Chen, H., Liu, M., and Liu, Z., 2013, Hierarchical Fe<sub>3</sub>O<sub>4</sub>@TiO<sub>2</sub> yolk-shell microspheres with enhanced microwave-absorption properties, *Chem. Eur. J.*, 19 (21), 6746–6752.
- [22] Zuas, O., Kim, J.S., and Gunlazard, J., 2014, Influence of operational parameters on the photocatalytic activity of powdered TiO<sub>2</sub> for the reduction of CO<sub>2</sub>, *Indones. J. Chem.*, 14 (2), 122–130.
- [23] Habisreutinger, S.N., Schmidt-Mende, L., and Stolarczyk, J.K., 2013, Photocatalytic reduction of CO<sub>2</sub> on TiO<sub>2</sub> and other semiconductors, *Angew. Chem. Int. Ed.*, 52 (29), 7372–7408.